JACS
JOURNAL OF THE AMERICAN CHEMICAL SOCIETY

COMMUNICATION

pubs.acs.org/JACS

Room-Temperature Electrochemical Reduction of Epitaxial Magnetite Films to Epitaxial Iron Films

Zhen He, Rakesh V. Gudavarthy, Jakub A. Koza, and Jay A. Switzer*

Department of Chemistry and Graduate Center for Materials Research, Missouri University of Science and Technology, Rolla, Missouri 65409-1170, United States

Supporting Information

ABSTRACT: The electrochemical reduction of oxides to metals has been studied for decades. Earlier work produced polycrystalline bulk metals. Here, we report that pre-electrodeposited epitaxial face-centered cubic magnetite thin films can be electrochemically reduced to epitaxial body-centered cubic iron thin films in aqueous solution on single-crystalline gold substrates at room temperature. This technique opens new possibilities to produce special epitaxial metal/metal oxide heterojunctions and a wide range of epitaxial metallic alloy films from the corresponding mixed metal oxides.

The electrochemical reduction of metal oxides to the corresponding metals has been studied for several decades as an alternative to pyrometallurgical processes for the metallurgy industry because of its simplicity, environmental friendliness, and low cost.[1−16] Fray and Chen pioneered this field with their work on the direct electrochemical reduction of titanium dioxide to titanium in molten calcium chloride at 950 °C.[3−6] Cox and Fray also showed that iron(III) oxide could be electrochemically reduced to iron in molten NaOH at 530 °C by the same method.[7] In recent work, Allanore and co-workers electrochemically reduced porous iron ore (α-Fe_2O_3, hematite) particles to iron in 10 M KOH solution at 100 °C. They proposed a dissolution/redeposition mechanism with magnetite (Fe_3O_4) as the intermediate.[8,9] In addition to TiO_2 and Fe_2O_3, more insulating oxides such as SiO_2 and ZrO_2 can also be reduced to Si and Zr, respectively.[10−13] Kang and co-workers showed that nanosize Cu particles can be fabricated by electrochemically reducing CuO nanoparticles in neutral solution at 300 K.[14] However, the previous work in this field was designed to achieve large-scale and high-rate metal production as well as low CO_2 emissions, and it was conducted on bulk polycrystalline metal oxides. Although single-crystal Bi_2S_3 and BiOCl were reported to be electrochemically reduced to Bi metal via an electron/proton transfer reaction at ambient temperature, there was no correlation between the initial orientation of the oxide crystals and the orientation of the metal crystallites after reduction.[15,16] That is, the order of the single crystals was lost after reduction. Here, we report that epitaxial face-centered cubic (fcc) Fe_3O_4 thin films on gold single-crystalline substrates can be electrochemically reduced to epitaxial body-centered cubic (bcc) Fe thin films in 2 M NaOH solution at room temperature.

Fe_3O_4 is a half-metallic metal oxide with the inverse spinel structure and a cubic lattice parameter a = 0.8396 nm (space group $Fd3m$). Its conductive nature makes it a good candidate to study the electrochemical reduction to Fe. The epitaxial transformation of fcc-Fe_3O_4 to bcc-Fe is interesting to study because a pure solid-state transformation would require an ordered atom rearrangement in a solid at low temperature, with a large volume shrinkage from fcc-Fe_3O_4 to bcc-Fe. Fe has a lattice parameter of a = 0.2866 nm (space group $Im3m$). The volume of one Fe_3O_4 unit cell is 0.5919 nm^3, containing 24 Fe atoms that can form 12 unit cells of bcc-Fe with a total volume of 0.2825 nm^3. Thus, the transformation from fcc-Fe_3O_4 to bcc-Fe will cause a 52.3% shrinkage in volume. Considering the large volume change during the transformation and the low ion mobility in solids at low temperature, it is surprising that the Fe films reduced from the precursor Fe_3O_4 layers are still epitaxial.

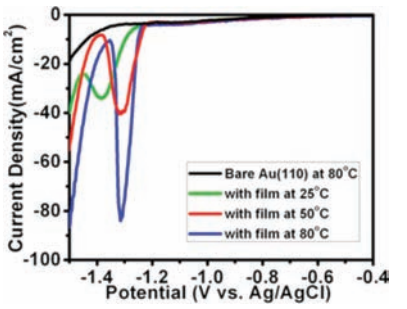

Figure 1. Linear sweep voltammograms on a bare Au(110) single crystal and on Au(110) with predeposited Fe_3O_4 films. All the voltammograms were run at a scan rate of 25 mV/s and stirring rate of 200 rpm in 2 M NaOH.

The electrochemical reduction of Fe_3O_4 to Fe was studied at temperatures ranging from 25 to 80 °C by linear sweep voltammetry (LSV). The potential was scanned from the open circuit potential to −1.5 V vs Ag/AgCl on the predeposited 200 nm thick Fe_3O_4 films[17] on a Au(110) single crystal and on a bare Au(110) single crystal in 2 M NaOH solution (see Figure 1). The LSV on the bare Au(110) shows only the cathodic current for water reduction starting at a potential of about −1.35 V vs Ag/AgCl. The potential at which water reduction occurs on both the bare Au electrode and the Fe_3O_4 electrodes is shifted to more negative potentials than the thermodynamic potential due to a kinetic overpotential. The LSVs on the predeposited Fe_3O_4 films on Au(110) all have one cathodic peak before water reduction which is due to the reduction of the Fe_3O_4 films. The reduction of

Received: April 29, 2011
Published: July 14, 2011

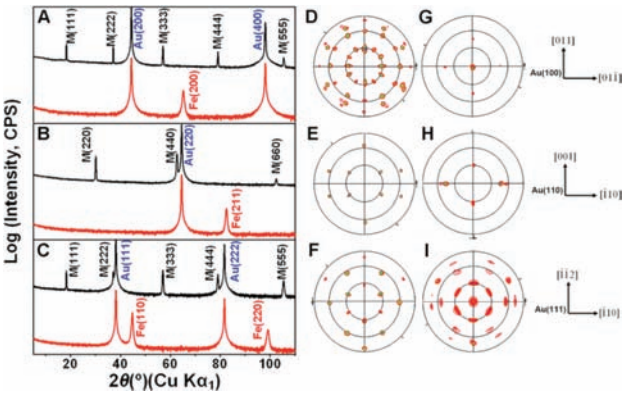

Figure 2. X-ray diffraction characterization of electrodeposited Fe_3O_4 films and the corresponding Fe films electrochemically reduced from the precursor Fe_3O_4 films. Left: $\theta-2\theta$ scans of Fe_3O_4 and Fe films on (A) Au(100), (B) Au(110), and (C) Au(111). Black lines represent scans on Fe_3O_4, and red lines represent scans on Fe films. The symbol "M" in this figure represents magnetite (Fe_3O_4). Middle: (311) pole figures of the Fe_3O_4 films on (D) Au(100), (E) Au(110), and (F) Au(111). Right: (110) pole figures of Fe on (G) Au(100) and (H) Au(110), and (I) (211) pole figure of Fe on Au(111).

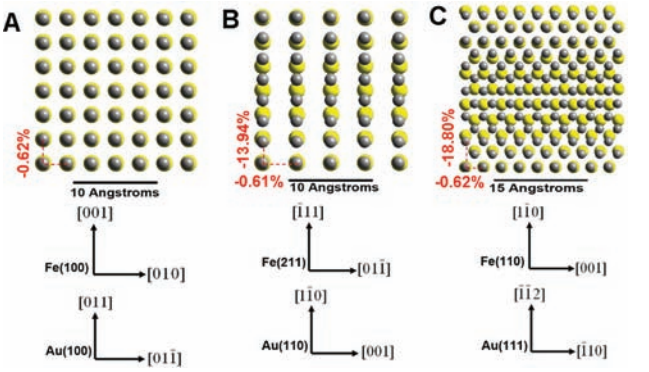

Figure 3. Interface models of the Fe films reduced from the precursor Fe_3O_4 films on (A) Au(100), (B) Au(110), and (c) Au(111). The yellow balls represent Au atoms, while the gray balls on the top represent Fe atoms.

Fe_3O_4 begins at about −1.20 V at all the temperatures. Based on these LSVs, the films were electrochemically reduced by applying −1.22 V vs Ag/AgCl. This potential is on the positive edge of the cathodic peaks for film reduction. The cathodic current density was typically 1−2 mA/cm^2 for reduction at 25 °C. If the films were reduced using the potentials corresponding to the peak currents (e.g., −1.4 V vs Ag/AgCl at 25 °C), the rapid film reduction led to exfoliation of the film.

The out-of-plane orientations of the predeposited Fe_3O_4 films (about 600 nm thick) and the Fe films (about 200 nm thick) electrochemically reduced from the precursor Fe_3O_4 films by applying a constant potential of −1.22 V vs Ag/AgCl were determined by X-ray diffraction (XRD) $\theta-2\theta$ scans. Plots of the logarithm of intensity versus 2θ for the precursor Fe_3O_4 films (black line) and the Fe films (red line) on Au(100), Au(110), and Au(111) single-crystalline substrates are shown in Figure 2A−C. As we showed in previous work,[18,19] Fe_3O_4 films grow with a [111] out-of-plane orientation on both Au(100) and Au(111) and a [110] out-of-plane orientation on Au(110). The out-of-plane orientations of the Fe films after reduction are [100] on Au(100), [110] on Au(111), and [211] on Au(110). Different out-of-plane orientations of the Fe films were obtained on Au(100) and Au(111) after reduction, whereas the precursor Fe_3O_4 films have the same out-of-plane orientation. Hence, the orientations of the Fe films are controlled by the Au substrates instead of the precursor Fe_3O_4 films. This suggests that the reduction starts at the Fe_3O_4/Au interface. Control of the orientations of both Fe_3O_4 and Fe layers by the Au substrates is an interesting phenomenon that might be applicable to produce special Fe_3O_4/Fe heterojunctions by partially reducing the precursor Fe_3O_4 films (Supporting Information (SI) Figure S2), which are not likely obtainable by other direct deposition techniques, because the orientation of the upper layer is usually controlled by the directly contacted bottom layer (SI Figure S1).

Texture analysis was used in order to probe the in-plane orientations of the precursor Fe_3O_4 films and the Fe films after reduction on all three Au single crystals. The (311) pole figures of the precursor Fe_3O_4 films on Au single crystals are shown in Figure 2D−F. The pole figures demonstrate that the Fe_3O_4 films were epitaxially deposited on all three Au single crystals.[18] The pole figures of both the Fe_3O_4 precursor films and the Fe films after electrochemical reduction have spot patterns instead of ring patterns, showing that the films have both out-of-plane and in-plane order. The epitaxial relationships are determined by comparing the experimentally measured pole figures to calculated stereographic projections (SI Figure S3). The (110) pole figure of the Fe film on Au(100) in Figure 2G shows that the epitaxial relationship for the Fe film on Au(100) is Fe(100)-[001]//Au(100)[011]. The (110) pole figure of Fe (Figure 2H) on Au(110) shows that there are two Fe domains on Au(110): Fe(211)[01$\bar{1}$]//Au(110)[001] and Fe(211)[0$\bar{1}$1]//Au(110)-[00$\bar{1}$]. The (211) pole figure of Fe film on Au(111) shown in Figure 2I shows that there are three domains of Fe film on the Au(111) substrate: Fe(110)[1$\bar{1}$0]//Au(111)[$\bar{1}\bar{1}$2], Fe(110)-[1$\bar{1}$0]//Au(111)[2$\bar{1}\bar{1}$], and Fe(110)[1$\bar{1}$0]//Au(111)[$\bar{1}$2$\bar{1}$].

The lattice mismatch between the Fe films and the Au single-crystalline substrates can be calculated on the basis of the Fe/Au interface models shown in Figure 3, which were generated according to the epitaxial relationships obtained from the XRD $\theta-2\theta$ scans and pole figure measurements. As shown in Figure 3A, on Au(100), the Fe(100) film and the Au(100) substrate have only −0.62% lattice mismatch along both Au[011] and Au[01$\bar{1}$] directions. However, on Au(110), the lattice mismatches of the Fe(211) and the Au(110) planes are −13.94% and −0.61% along the two orthogonal Au[1$\bar{1}$0] and [001] directions (Figure 3B). The situation on Au(111) is similar to that on Au(110). The Fe(110) and Au(111) planes have a small mismatch of −0.62% along Au[$\bar{1}$10] and a large mismatch of −18.80% along Au[$\bar{1}\bar{1}$2]. Therefore, the sequence of the lattice mismatches of Fe films on Au single crystals from small to large is Fe(100) on Au(100) < Fe(211) on Au(110) < Fe(110) on Au(111).

Another way to determine whether the reduction of Fe_3O_4 to Fe starts at the Au/Fe_3O_4 interface or at the Fe_3O_4/electrolyte interface is direct observation based on cross-sectional scanning electron microscopy (SEM) images and plan-view photomicrographs of a partially reduced Fe_3O_4 film on Au. The cross-sectional SEM image of the Fe_3O_4 film before partial reduction (Figure 4a) on an Au-sputtered glass substrate shows that the Fe_3O_4 film (top layer) has a columnar structure and the bright Au layer has a thickness of about 100 nm, which matches with the manufacturer's description. After partial reduction (Figure 4B),

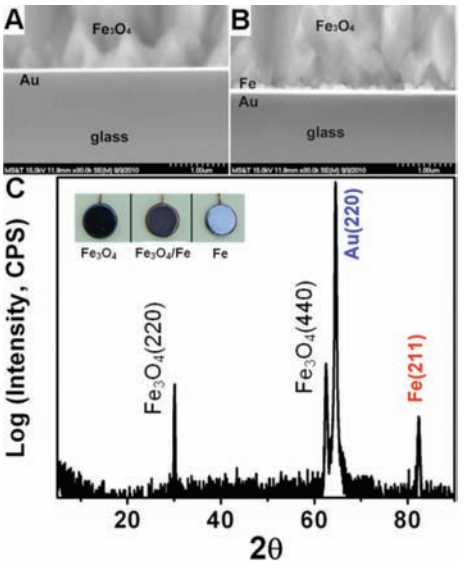

Figure 4. Evidence that the reduction of Fe_3O_4 to Fe starts at the Fe_3O_4/Au interface. SEM cross-sectional images of precursor Fe_3O_4 film on Au-sputtered glass (A) before and (B) after partial reductions. (C) XRD $\theta-2\theta$ scan of partially reduced Fe_3O_4 film on a Au(110) single crystal. The insets in (C) are plan-view photographs of the as-deposited Fe_3O_4 film (left), the partially reduced Fe_3O_4 film (middle), and the Fe film (right) completely reduced from the Fe_3O_4 film on Au(110).

the upper Fe_3O_4 layer and the Au layer are unchanged. Between the Au and Fe_3O_4 layers, a layer of Fe nanoparticles with a thickness of about 100−150 nm can be seen. The insets in Figure 4C are plan-view photographs of the as-deposited magnetite film, partially reduced magnetite film, and Fe film after complete reduction. The surface of the electrodeposited Fe_3O_4 film on Au(110) appears black, with a crystal size of 200−300 nm (as shown in SI Figure S4). After partial reduction, the XRD $\theta-2\theta$ scan (Figure 4C) confirms that part of the precursor Fe_3O_4(110) film has been reduced to an Fe(211) film. However, the photograph of the partially reduced magnetite film shows no obvious change of the Fe_3O_4 film surface. After complete reducition at room temperature until the cathodic current reached a plateau, there was a very thin layer of brownish-black film loosely attached to the surface that could be easily removed by flushing with distilled water. XRD and Raman analysis of this surface film show that it is Fe_3O_4, but the grain size measured by SEM is larger than that of the initial Fe_3O_4. After the top unreduced layer was removed, the Fe film with a shiny metallic gloss was exposed, with a crystal size around 100−150 nm based on the SEM image (SI Figure S4). These direct observations suggest that the reduction of Fe_3O_4 to Fe does not start at the Fe_3O_4/electrolyte interface but, rather, at the Fe_3O_4/Au interface, which agrees with the indirect deduction based on the X-ray characterization results.

In order to further analyze the Fe reduction product, magnetic investigations were performed. Hysteresis loops of the as-deposited Fe_3O_4 thin film as well as the Fe layer obtained after the reduction on the Au(110) crystal are shown in Figure 5. For both of the films, the easy axis of magnetization lies in the film plane. From the hysteresis loops obtained normal to the film plane, anisotropy fields have been estimated (indicated by arrows in Figure 5) to be ∼0.55 and ∼1.7 T for as-deposited Fe_3O_4 and Fe

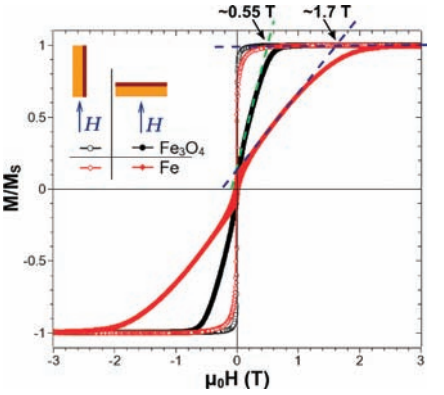

Figure 5. Normalized magnetization vs magnetic field hysteresis loops of the as-deposited Fe_3O_4 film and the Fe film reduced from the precursor Fe_3O_4 film on a single-crystal Au(110) substrate.

films, respectively. The value for the Fe_3O_4 film is very close to the saturation magnetization of Fe_3O_4, indicating a predominant contribution of shape anisotropy, as already reported by other researchers.[20] The hysteresis loop for the Fe film has a significantly larger anisotropy field than Fe_3O_4. The estimated anisotropy field is very close to the saturation magnetization of pure Fe, which further proves that the reduction product is Fe. Additionally, as mentioned, Fe_3O_4/Fe heterostructures with different epitaxial relationships can be formed, which may show interesting exchange coupling phenomena.

From our experiments it is not possible to determine whether the reduction of Fe_3O_4 to Fe occurs by a solid-state transformation or through a dissolution/redeposition route. The fact that the reaction occurs at the Au/Fe_3O_4 interface suggests a solid-state transformation, whereas the large currents observed in Figure 1 are more consistent with the dissolution/redeposition route. The solid-state transformation would occur by reducing Fe_3O_4 to Fe and O^{2-} (eq 1). The O^{2-} would then be transported to the surface (eq 2), where it would react with H_2O to produce OH^-(eq 3).

$$Fe_3O_4 + 8e^- \leftrightarrows 3Fe + 4O^{2-}_{bulk} \quad (1)$$

$$4O^{2-}_{bulk} \leftrightarrows 4O^{2-}_{surface} \quad (2)$$

$$4O^{2-}_{surface} + 4H_2O \leftrightarrows 8OH^- \quad (3)$$

However, the diffusion coefficient of O^{2-} in magnetite would be exceedingly small at room temperature, because it has been measured[21] to be 5.6×10^{-19} cm^2/s at 500 °C, compared with values in the 10^{-6} cm^2/s range for aqueous ions. Of course, transport of O^{2-} along grain boundaries or in nanophase material at the Au/Fe_3O_4 interface could be much faster than the previously measured bulk values. It is also possible that the O^{2-} ions do not need to diffuse through the entire film, but they can be released directly into electrolyte that has infiltrated through the capillaries between the columnar grains of Fe_3O_4. This would be in line with the three-phase interlines model.[5,22,23] The dissolution/redeposition route is consistent with the mechanism proposed by Allanore et al. for reduction of Fe_2O_3 in strongly alkaline solution, with Fe_3O_4 as an intermediate.[8,9] This route would occur according to eqs 4 and 5. In this case the Fe_3O_4 is electrochemically reduced to a soluble Fe(II) species such as $Fe(OH)_3^-$, which is then reduced at the Au electrode to Fe.

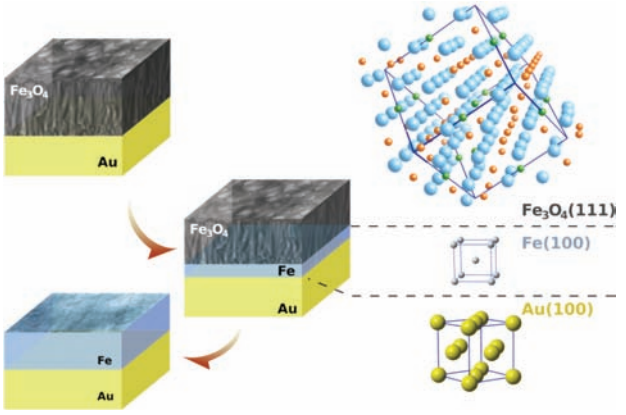

Figure 6. Scheme for the reduction of epitaxial Fe_3O_4 film to epitaxial Fe film on an Au single-crystalline substrate. The reduction of Fe_3O_4-(111) to Fe(100) on Au(100) is shown as an example.

Again, for this mechanism to explain the deposition of Fe at the Au surface, it is necessary to invoke the concept of infiltration of electrolyte into the film.

$$Fe_3O_4 + 2e^- + 4H_2O + OH^- \leftrightarrows 3Fe(OH)_3^- \quad (4)$$

$$3Fe(OH)_3^- + 6e^- \leftrightarrows 3Fe + 9OH^- \quad (5)$$

In addition to Fe_3O_4-to-Fe conversion, our preliminary experimental results also showed that alloy films with a controlled metal ratio can be produced by electrochemical reduction of the corresponding mixed metal oxide films. We electrochemically reduced a cobalt-substituted Fe_3O_4 film and measured the cobalt concentrations in both the precursor oxide film and the metallic film after reduction. The results show that the atomic cobalt concentrations are 16.2% in the precursor oxide film and 16.0% in the metallic film after reduction, with the XRD pattern of the metallic film after reduction matching that of the CoFe alloy. This indicates that the metals' concentration ratio in the alloy film can be determined by the ratio in the precursor mixed metal oxide film.

We have shown that epitaxial Fe_3O_4 films on single-crystal Au can be electrochemically reduced to epitaxial Fe films that maintain the single-crystal-like order of the Fe_3O_4 precursor (see scheme in Figure 6). The reduction starts at the Fe_3O_4/Fe interface instead of the Fe_3O_4/solution interface, with the orientation of the resulting Fe film determined by the Au substrate. In addition to producing pure Fe films, we have shown that Fe_3O_4/Fe heterojunctions can be produced by partially reducing the Fe_3O_4, and that Fe/Co alloys can be produced from cobalt-substituted Fe_3O_4. The method should be quite general. For example, we anticipate that it should be possible to reduce epitaxial films of other metal oxides such as Bi_2O_3,[15,24,25] Cu_2O,[26] and CuO[27] to the corresponding epitaxial metals. Because the orientations of the films are determined by the single-crystal substrate, it is interesting to speculate whether amorphous films of SiO_2 could be reduced in nonaqueous solvents or molten salts to epitaxial films of Si on ordered substrates.[10−12] This would provide an inexpensive method to produce large-scale epitaxial Si films for electronic and photovoltaic applications.

■ ASSOCIATED CONTENT

Supporting Information. Experimental details. This material is available free of charge via the Internet at http://pubs.acs.org.

■ AUTHOR INFORMATION

Corresponding Author
jswitzer@mst.edu

■ ACKNOWLEDGMENT

This work was supported by the U.S. Department of Energy, Office of Basic Energy Sciences, under Grant No. DE-FG02-08ER46518.

■ REFERENCES

(1) Oswin, H. G.; Cohen, M. *J. Electrochem. Soc.* **1957**, *104*, 9.
(2) LeDuc, J. A. M.; Loftfield, R. E.; Vaaler, L. E. *J. Electrochem. Soc.* **1959**, *106*, 659.
(3) Chen, G. Z.; Fray, D. J.; Farthing, T. W. *Nature* **2000**, *407*, 361.
(4) Jiang, K.; Hu, X.; Ma, M.; Wang, D.; Qiu, G.; Jin, X.; Chen, G. Z. *Angew. Chem., Int. Ed.* **2006**, *45*, 428.
(5) Li, W.; Jin, X.; Huang, F.; Chen, G. Z. *Angew. Chem., Int. Ed.* **2010**, *49*, 3203.
(6) Centeno-Sanchez, R. L.; Fray, D. J.; Chen, G. Z. *J. Mater. Sci.* **2007**, *42*, 7494.
(7) Cox, A.; Fray, D. J. *J. Appl. Electrochem.* **2008**, *38*, 1401.
(8) Allanore, A.; Lavelaine, H.; Valentin, G.; Birat, J. P.; Delcroix, P.; Lapicque, F. *Electrochim. Acta* **2010**, *55*, 4007.
(9) Allanore, A.; Lavelaine, H.; Valentin, G.; Birat, J. P.; Lapicque, F. *J. Electrochem. Soc.* **2008**, *155*, E125.
(10) Nohira, T.; Yasuda, K.; Ito, Y. *Nat. Mater.* **2003**, *2*, 397.
(11) Jin, X.; Gao, P.; Wang, D.; Hu, X.; Chen, G. Z. *Angew. Chem., Int. Ed.* **2004**, *43*, 733.
(12) Xiao, W.; Jin, X.; Deng, Y.; Wang, D.; Chen, G. Z. *J. Electroanal. Chem.* **2010**, *639*, 130.
(13) Peng, J.; Jiang, K.; Xiao, W.; Wang, D.; Jin, X.; Chen, G. Z. *Chem. Mater.* **2008**, *20*, 7274.
(14) Han, W.-K.; Choi, J.-W.; Hwang, G.-H.; Hong, S.-J.; Lee, J.-S.; Kang, S.-G. *Appl. Surf. Sci.* **2006**, *252*, 2832.
(15) Pyper, O.; Hahn, B.; Schoellhorn, R. *J. Mater. Chem.* **1997**, *7*, 465.
(16) Pfletschinger, G.; Hahn, B.; Schoellhorn, R. *Solid State Ionics* **1996**, *84*, 151.
(17) Kothari, H. M.; Kulp, E. A.; Limmer, S. J.; Poizot, P.; Bohannan, E. W.; Switzer, J. A. *J. Mater. Res.* **2006**, *21*, 293.
(18) Kulp, E. A.; Kothari, H. M.; Limmer, S. J.; Yang, J.; Gudavarthy, R. V.; Bohannan, E. W.; Switzer, J. A. *Chem. Mater.* **2009**, *21*, 5022.
(19) Switzer, J. A.; Gudavarthy, R. V.; Kulp, E. A.; Mu, G.; He, Z.; Wessel, A. J. *J. Am. Chem. Soc.* **2010**, *132*, 1258.
(20) Horng, L.; Chern, G.; Chen, M. C.; Kang, P. C.; Lee, D. S. *J. Magn. Magn. Mater.* **2004**, *270*, 389.
(21) Castle, J. E.; Surman, P. L. *J. Phys. Chem.* **1967**, *71*, 4255.
(22) Deng, Y.; Wang, D.; Xiao, W.; Jin, X.; Hu, X.; Chen, G. Z. *J. Phys. Chem. B* **2005**, *109*, 14043.
(23) Xiao, W.; Jin, X.; Deng, Y.; Wang, D.; Chen, G. Z. *Chem.—Eur. J.* **2007**, *13*, 604.
(24) Switzer, J. A.; Shumsky, M. G.; Bohannan, E. W. *Science* **1999**, *284*, 293.
(25) Qiu, Y.; Liu, D.; Yang, J.; Yang, S. *Adv. Mater.* **2006**, *18*, 2604.
(26) Switzer, J. A.; Hung, C. J.; Bohannan, E. W.; Shumsky, M. G.; Golden, T. D.; Van Aken, D. C. *Adv. Mater.* **1997**, *9*, 334.
(27) Switzer, J. A.; Kothari, H. M.; Poizot, P.; Nakanishi, S.; Bohannan, E. W. *Nature* **2003**, *425*, 490.